Supporting Information for

Constructing four-in-one catalysts to realize ultralow voltage hydrogen production at ampere-level current densities

Minghui Xing[1], Mengting Han[1], Guoqing Xu[1], Zhiping Liu[1], Qinglan Zhao[2], Minhua Shao[2], Jimmy Yun[3,4], Peng Wang[5], Dapeng Cao[*1]

[1] *State Key Laboratory of Organic-Inorganic Composites, Beijing University of Chemical Technology, Beijing 100029, China.*

[2] *Department of Chemical and Biological Engineering, Hong Kong University of Science and Technology, Clear Water Bay, Kowloon, Hong Kong, China*

[3] *Qingdao International Academician Park Research Institute, Qingdao 266000, China;*

[4] *School of Chemical Engineering, The University of New South Wales, Sydney, NSW 2052, Australia.*

[5] *Qihang New Energy Technology Co. Ltd, China Railway Rolling Stock Corporation, Beijing 100039, China.*

**Corresponding Author. Email: caodp@buct.edu.cn*

Chemicals

Cobaltous Nitrate Hexahydrate ($CoH_{12}N_2O_{12}$, 99%), Ammonium metavanadate (NH_4VO_3, 99.95% metals basis), ammonium fluoride (NH_4F, 99.5%), Urea (CH_4N_2O, 99%), hydrazine hydrate ($N_2H_4 \cdot H_2O$, 80%), KOH and commercial Pt/C (RuO_2) were purchased from Aladdin (Shanghai, China). Ni foam (NF) (2*4 cm^2) was pretreated in 3 M HCl by ultrasonic treatment for 20 min.

Preparation of V-Co(OH)$_2$. Typically, $CoH_{12}N_2O_{12}$ (524.0 mg, 2.2 mmol), NH_4VO_3 (35.1 mg, 0.3 mmol), NH_4F (148.0 mg, 4.0 mmol), and CH_4N_2O (450.0 mg, 7.5 mmol) were dissolved in 30 ml deionized water. After that, a piece of nickel foam (2*4 cm^2) was placed in above precursor solution in a teflon-lined autoclave (50 mL), followed by heating the solution at 120 °C for 6 h. The product was then rinsed several times with deionized water and ethanol to remove the surface loaded samples, and the as-prepared catalyst was washed with water and dried under Ar.

Preparation of V_{SA}-CoN_X. For preparing V_{SA}-CoN_X, the V-Co(OH)$_2$ (2*4 cm^2) was put in the tubular furnace was heated to 500 °C with a heating rate of 5 °C min^{-1} and maintained for 2 h under an NH_3 flow.

Preparation of CoN_X. For preparing CoN_X, the preparation steps are identical except that NH_4VO_3 is not added to the hydrothermal process in the first step.

Characterizations

Powder X-ray diffraction (XRD) data was measured on a RigakuD/MAX 2550 diffractometer with Cu Kα radiation (λ = 1.5418 Å). ZEISS GeminiSEM 300 was used to acquire scanning electron microscopy (SEM) at an accelerating voltage of 3 kV. A

ThermoFisherESCALab 250 (ThermoFisher, E. Grinstead, UK) was performed to get the X-ray photoelectron spectroscopy (XPS) data, using Al Ka X-ray radiation for excitation. Energy dispersive X-ray spectroscopy (EDX) and high-resolution TEM (HRTEM) images were obtained by a FEI Tecnai G2 F30 at an accelerating voltage of 300 kV. Inductively coupled plasma optical emission spectroscopy (ICP-OES) was used to confirm the compositions of the samples.

Electrochemical measurements

All the catalytic measurements were performed with a CHI 760E electrochemistry workstation (CH Instruments, Inc., Shanghai) in a standard three-electrode system using V_{SA}-CoN_X as the working electrode, a graphite rod as the counter electrode and an Hg/HgO electrode as the reference electrode. As show in Figure S9, the zero point of RHE was calibrated using the HER/HOR equilibrium potential using Pt catalyst in H_2-saturated solutions (E_{RHE}=$E_{Hg/HgO}$+0.925), 1 M KOH (or 1 M KOH+0.5 M urea, or 1 M KOH+0.3 M N_2H_4) solution was used as electrolyte for HER, OER, UOR and HzOR. Linear sweep voltammetry (LSV) is recorded at a scan rate of 5 mV s^{-1}. Without explanation all polarization curves are 85% iR corrected by default and all the AEMWE device data are without iR corrected. The flow rate of the electrolyte in the AEMWE device was set to 100 ml/min and the text temperature of AEMWE is 70 °C.

***In-situ* Raman spectro-electrochemistry**

In-situ Raman measurements were performed with a custom-made spectro-electrochemical cell. The electrochemical activities were measured in a three-electrode configuration at room temperature. The as-obtained catalyst V_{SA}-CoN_X, Pt wire and

Hg/HgO were used as a working electrode, counter electrode, and reference electrode, respectively.

Measurement of Hydrazine Degradation Rate

Preconfigure solution A: 0.6 mol/L HCL. Solution B: 1g dimethylbenzaldehyde+50 mL ethanol+5ml concentrated hydrochloric acid.

During the process of testing the hydrazine concentration, first prepare the hydrazine standard, take 0, 0.24, 0.48, 0.72, 0.96, 1.4ug/ml of the prepared hydrazine standard solution for the calibration of the standard curve, and calculate the regression equation. Then, during the stability test, collect electrolyte regularly and quantitatively. The concentration of hydrazine was measured at λ = 457 nm using the UV–vis spectrum of the solution.

XANES measurements

The X-ray absorption spectra (XAS) including X-ray absorption near-edge structure (XANES) and extended X-ray absorption fine structure (EXAFS) of the samples were collected at the Singapore Synchrotron Light Source (SSLS) center, where a pair of channel-cut Si (111) crystals was used in the monochromator. The storage ring was working at the energy of 700 MeV with average electron current of below 200 mA.

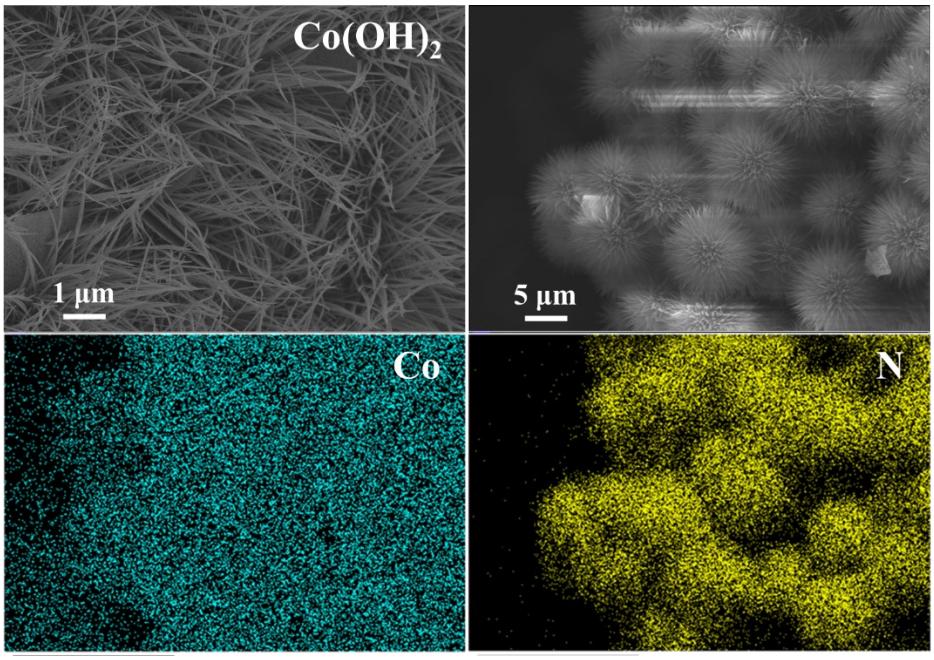

Figure S1. SEM image and EDS elemental mapping images of $Co(OH)_2$.

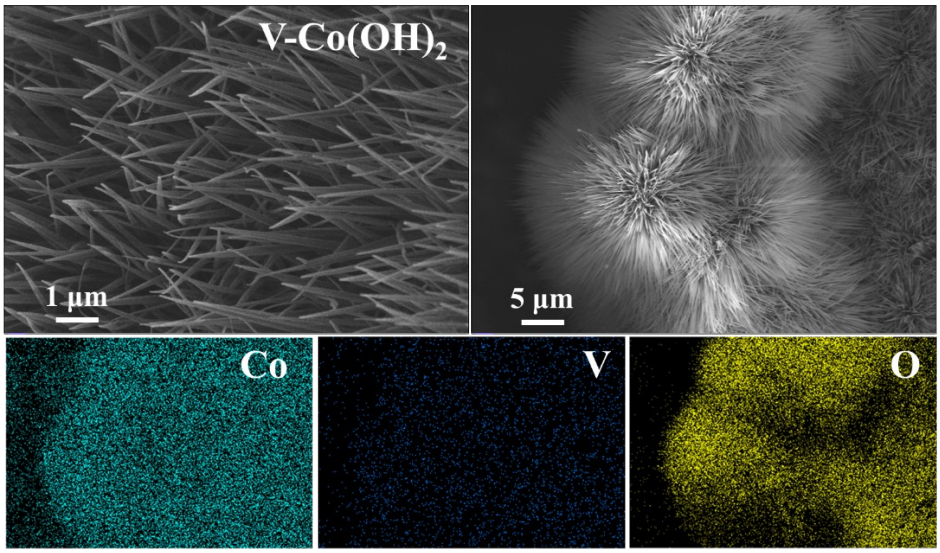

Figure S2. SEM image and EDS elemental mapping images of V-$Co(OH)_2$.

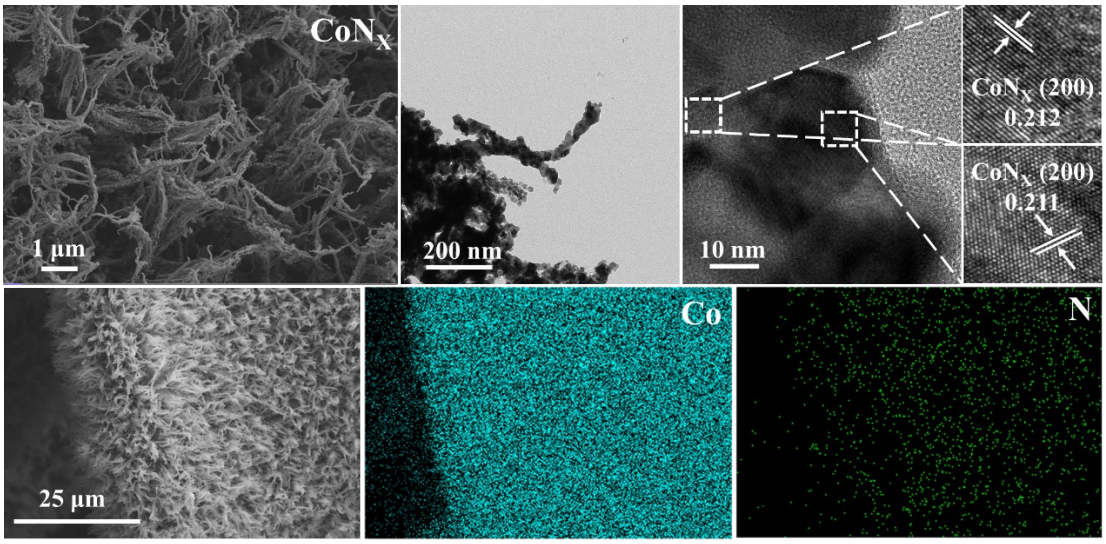

Figure S3. SEM, TEM images and EDS elemental mapping images of CoN_X.

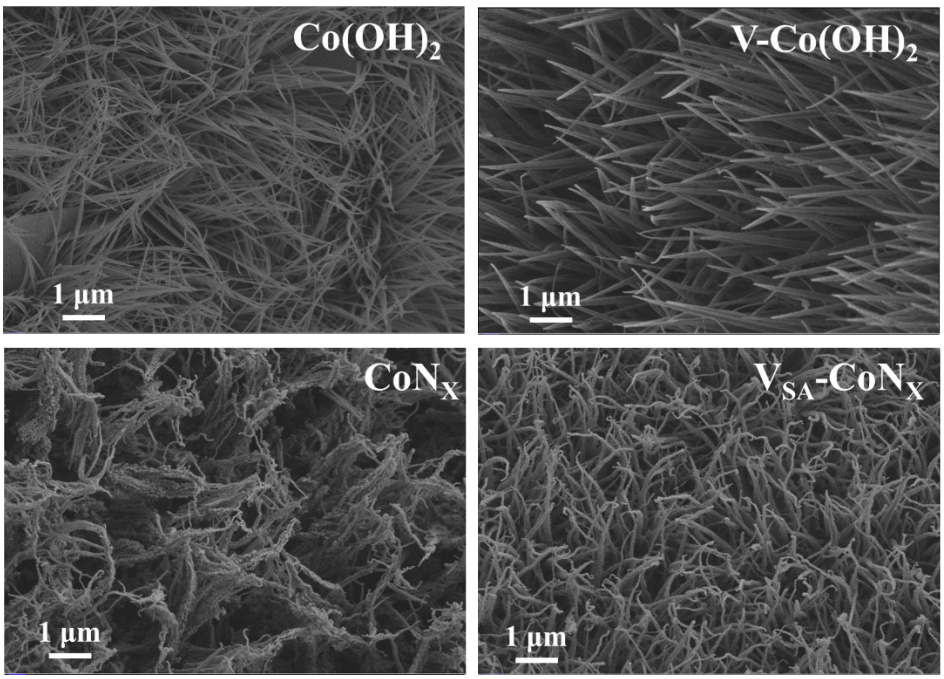

Figure S4. SEM images of $Co(OH)_2$, $Co(OH)_2$, CoN_X and V_{SA}-CoN_X.

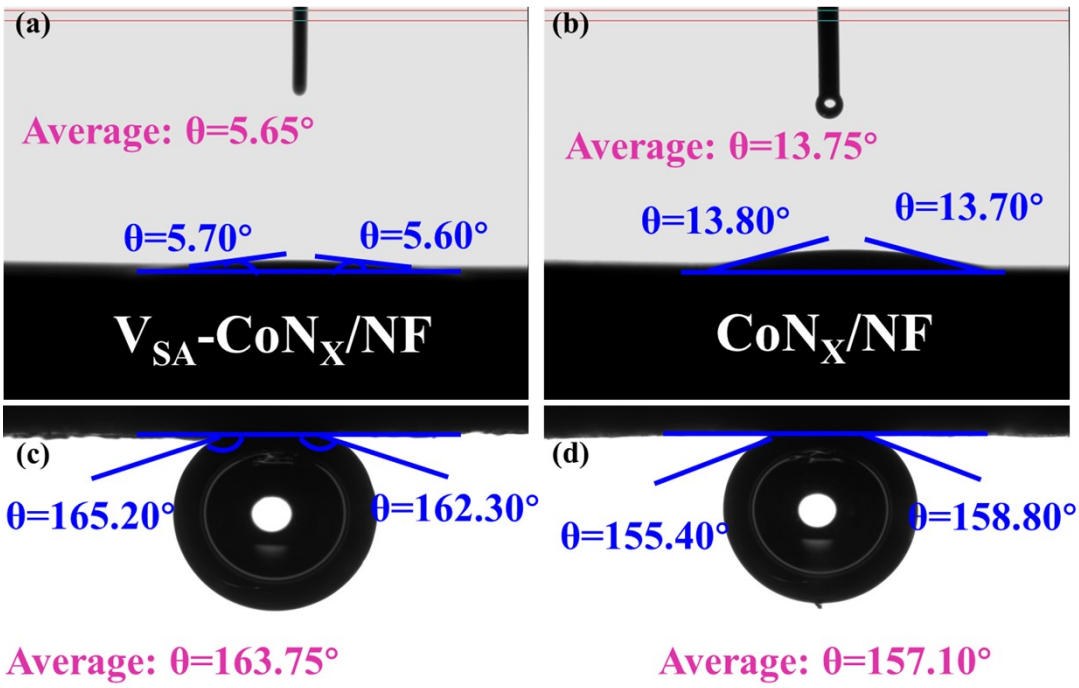

Figure S5. The contact angles of V_{SA}-CoN_X and CoN_X using the KOH electrolyte. Static droplets contact angles of a) V_{SA}-CoN_X and b) CoN_X. The air-bubble contact angles images of c) V_{SA}-CoN_X and d) CoN_X.

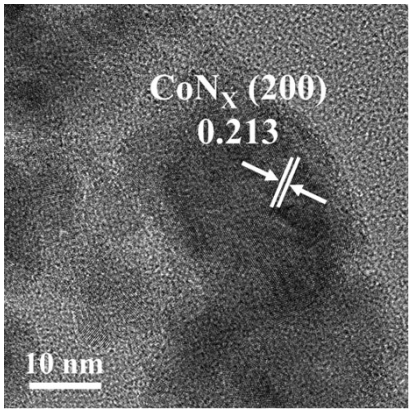

Figure S6. HRTEM image of V_{SA}-CoN_X.

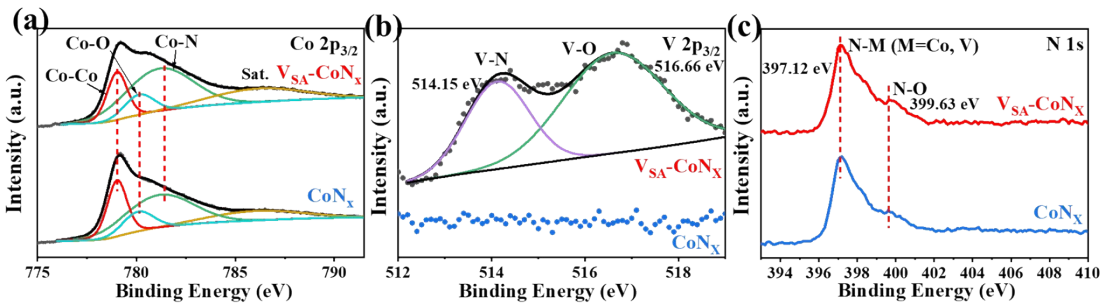

Figure S7. f) Co 2p3/2, g) V 2p3/2 and h) N 1s XPS spectra for V_{SA}-CoN_X and CoN_X.

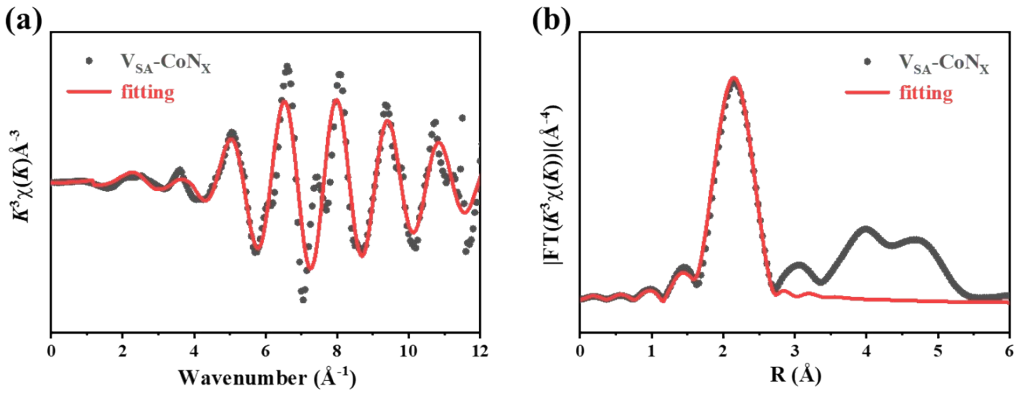

Figure S8. Fitting curves of the EXAFS of Co in V_{SA}-CoN_X in the a) K-space and b) R-space. c) The schematic diagram of V_{SA}-CoN_X. The blue, white and orange balls represent Co, N and V atom, respectively.

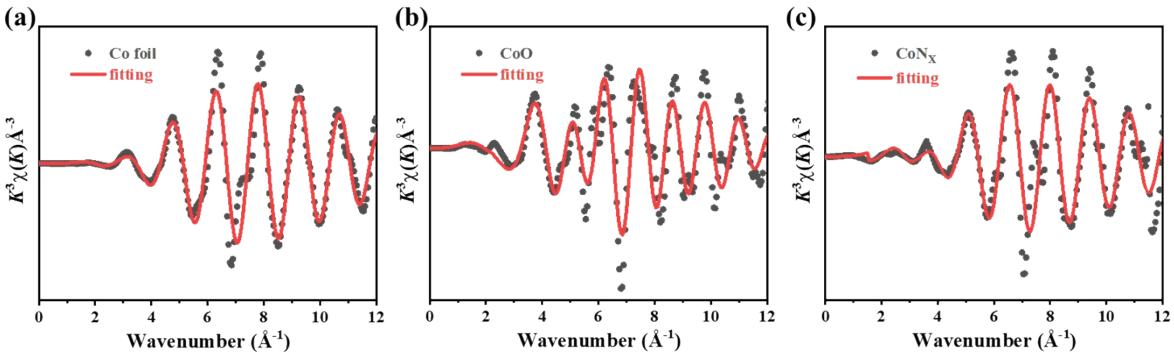

Figure S9. Fitting curves of the EXAFS of Co in the reference samples in the K-space.

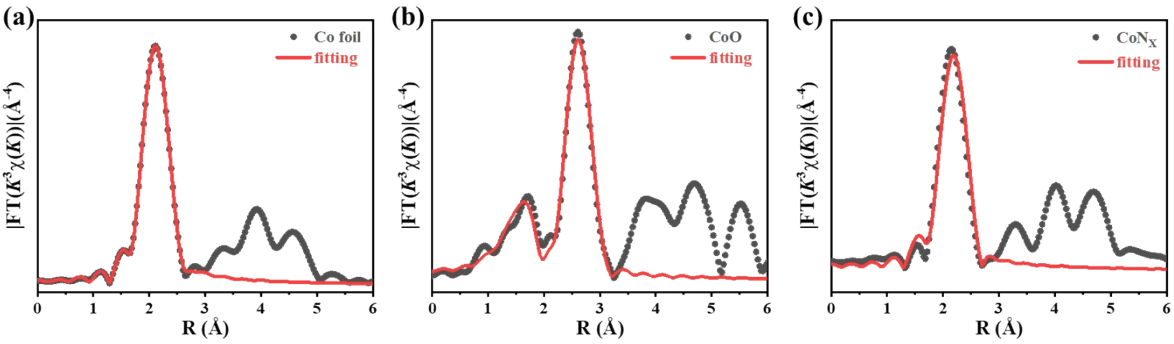

Figure S10. Fitting curves of the EXAFS of Co in the reference samples at the R-space.

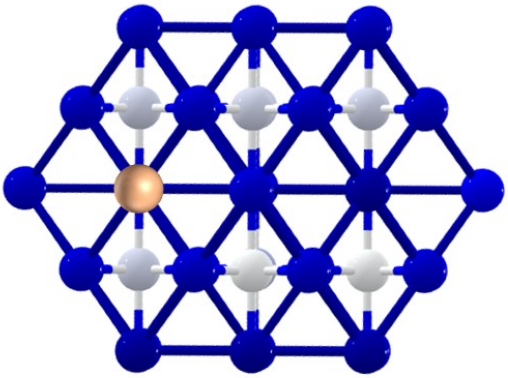

Figure S11. The schematic diagram of V_{SA}-CoN_X. The blue, white and orange balls represent Co, N and V atom, respectively.

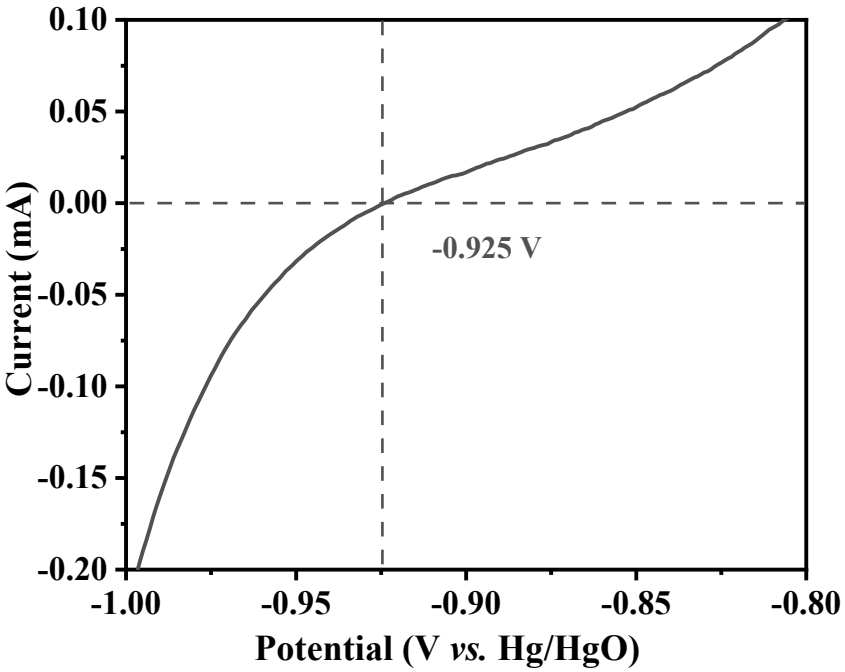

Figure S12. Current-potential curve of Pt wire in highly pure H_2-saturated 1 M KOH aqueous solution, used for calibration of the Ag/AgCl electrode with respect to RHE. Scan rate 1 mV s^{-1}. The potentials were calibrated to $E_{RHE}=E_{Hg/HgO}+0.925$.

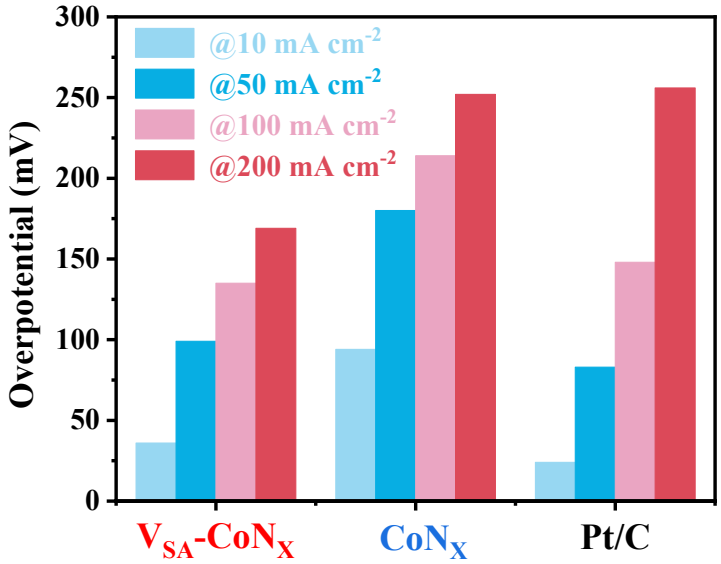

Figure S13.The overpotentials at 10, 50, 100 and 200 mA cm^{-2} for V_{SA}-CoN_X, CoN_X and Pt/C.

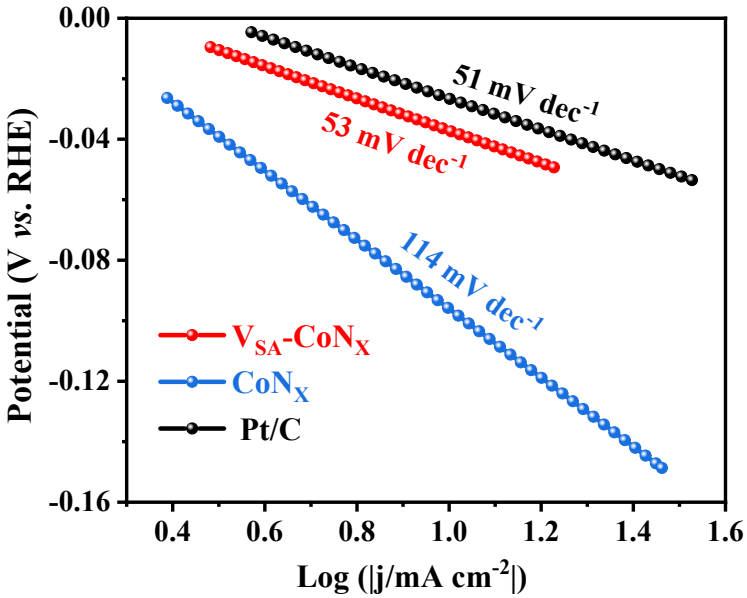

Figure S14. Tafel slope of V_{SA}-CoN_X, CoN_X and Pt/C.

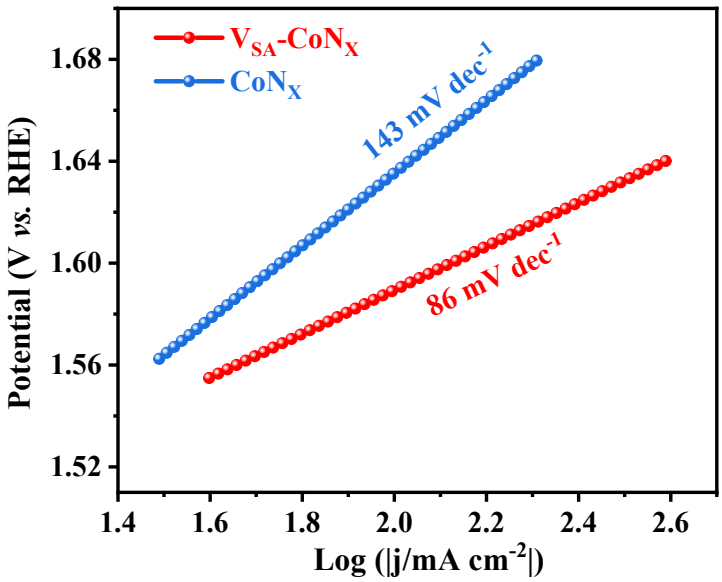

Figure S15. Tafel slope of V_{SA}-CoN_X and CoN_X for OER.

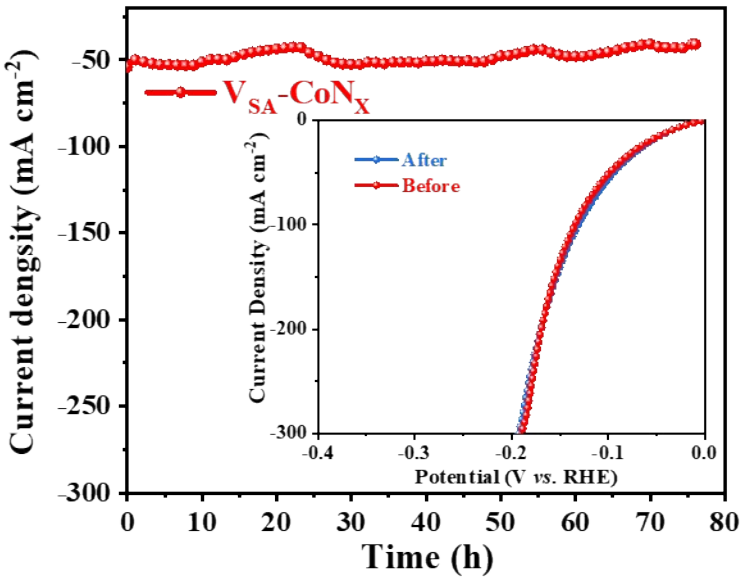

Figure S16. The long-term stability of V_{SA}-CoN_X for HER (inset is the polarization curves before and after the stability test)

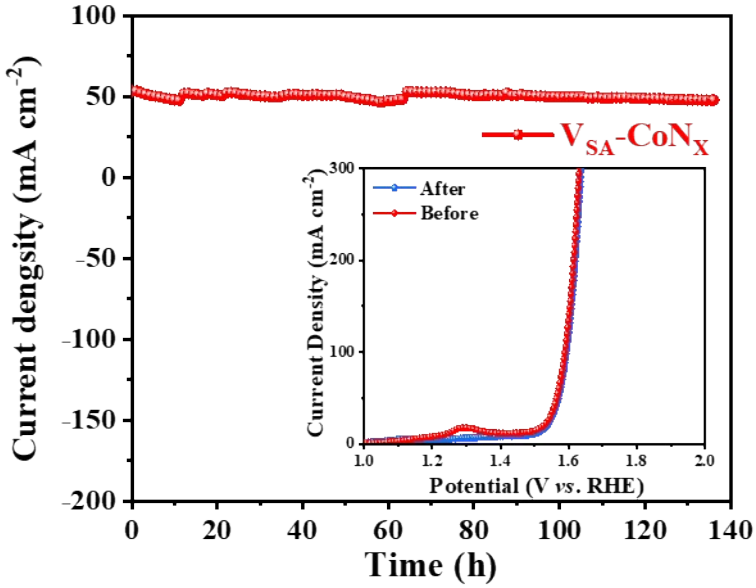

Figure S17. The long-term stability of V_{SA}-CoN_X for OER (inset is the polarization curves before and after the stability test)

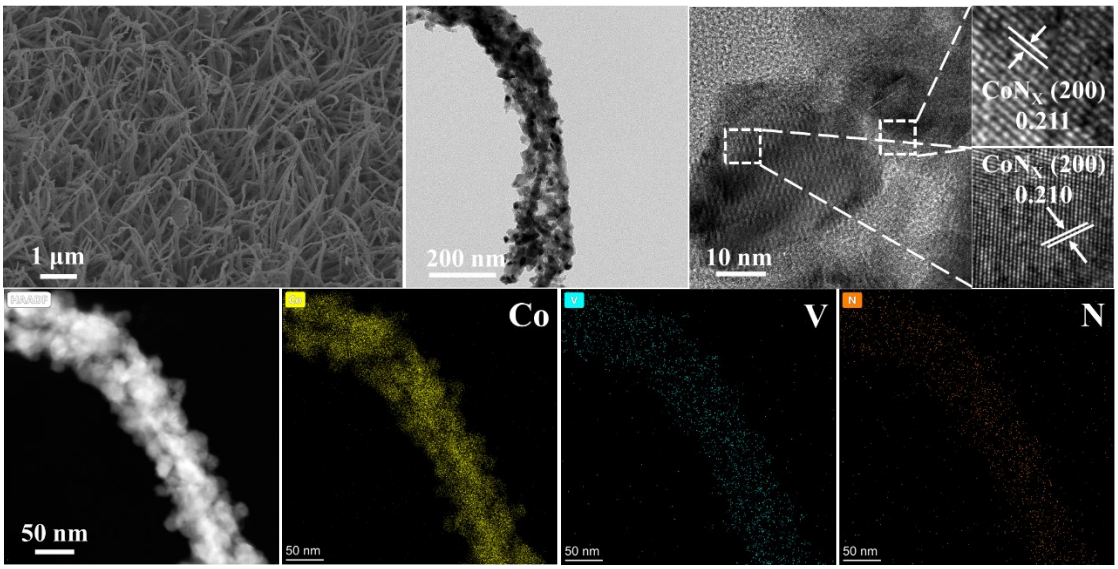

Figure S18. Characterizations of V_{SA}-CoN_X after HER stability test.

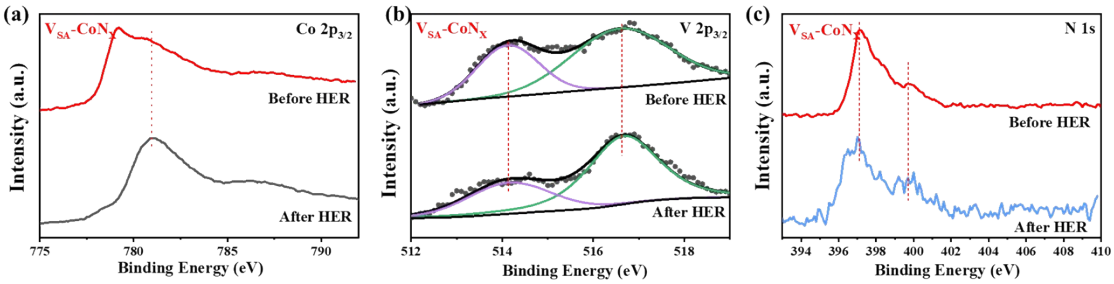

Figure S19. XPS of V_{SA}-CoN_X before and after HER stability test.

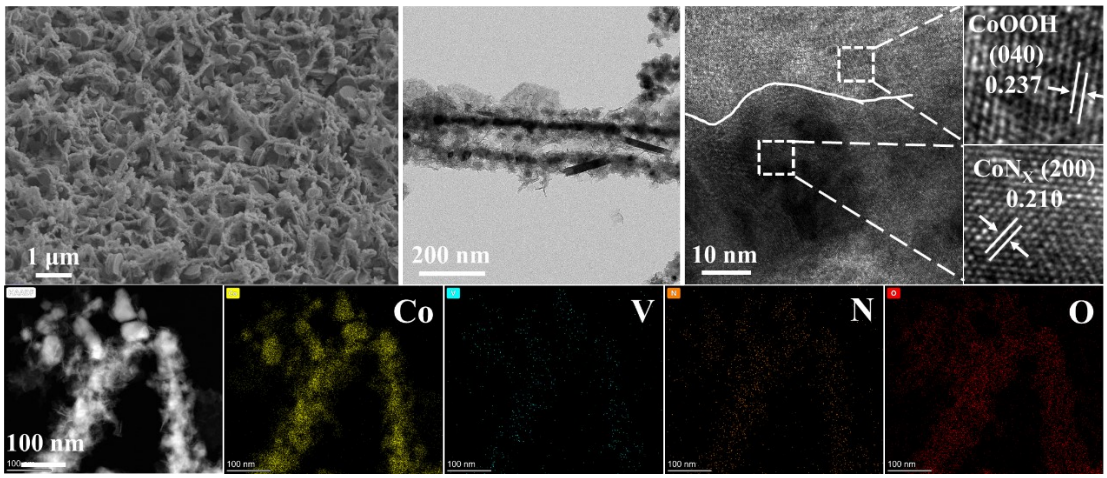

Figure S20. Characterizations of V_{SA}-CoN_X after OER stability test.

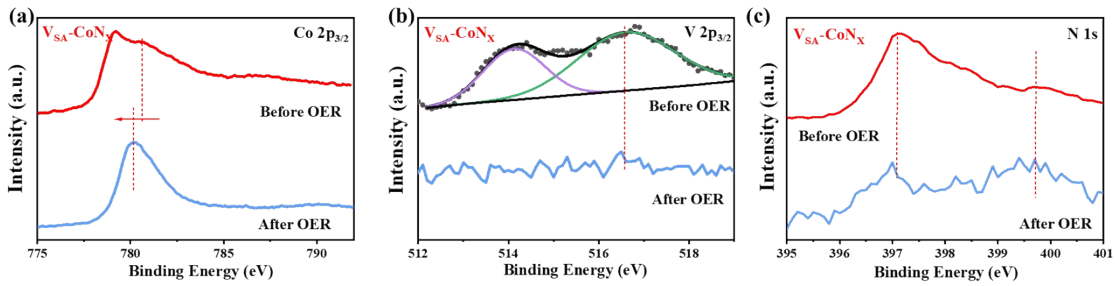

Figure S21. XPS of V_{SA}-CoN_X before and after OER stability test.

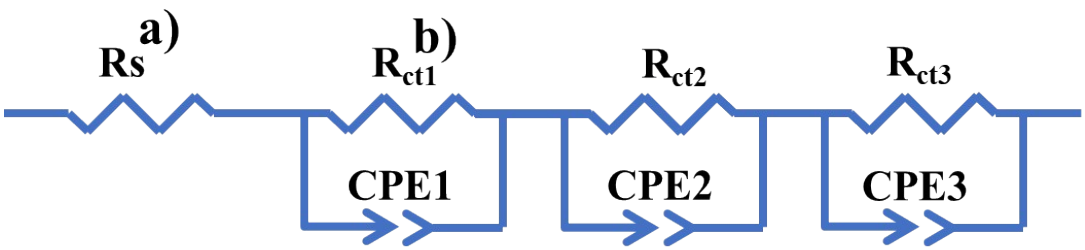

Figure S22. The equivalent circuit for modeling the measured electrochemical response in 1 M KOH for HER.

a) R_s represents solution resistance;

b) R_{ct} represents charge transfer resistance.

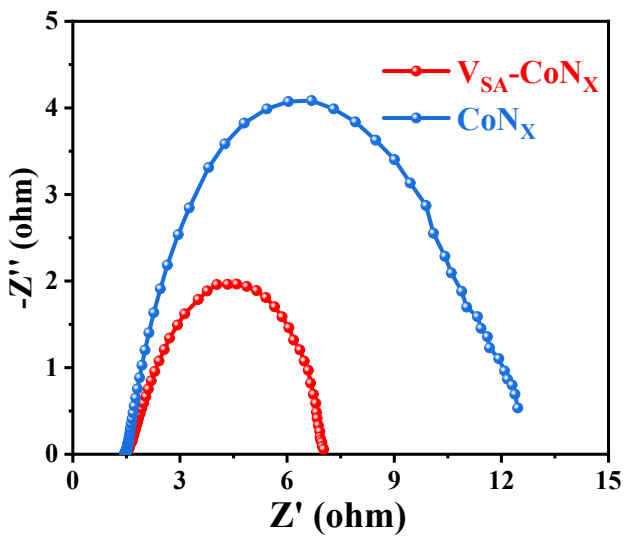

Figure S23. Nyquist plots of V_{SA}-CoN_X and CoN_X at -0.075 V.

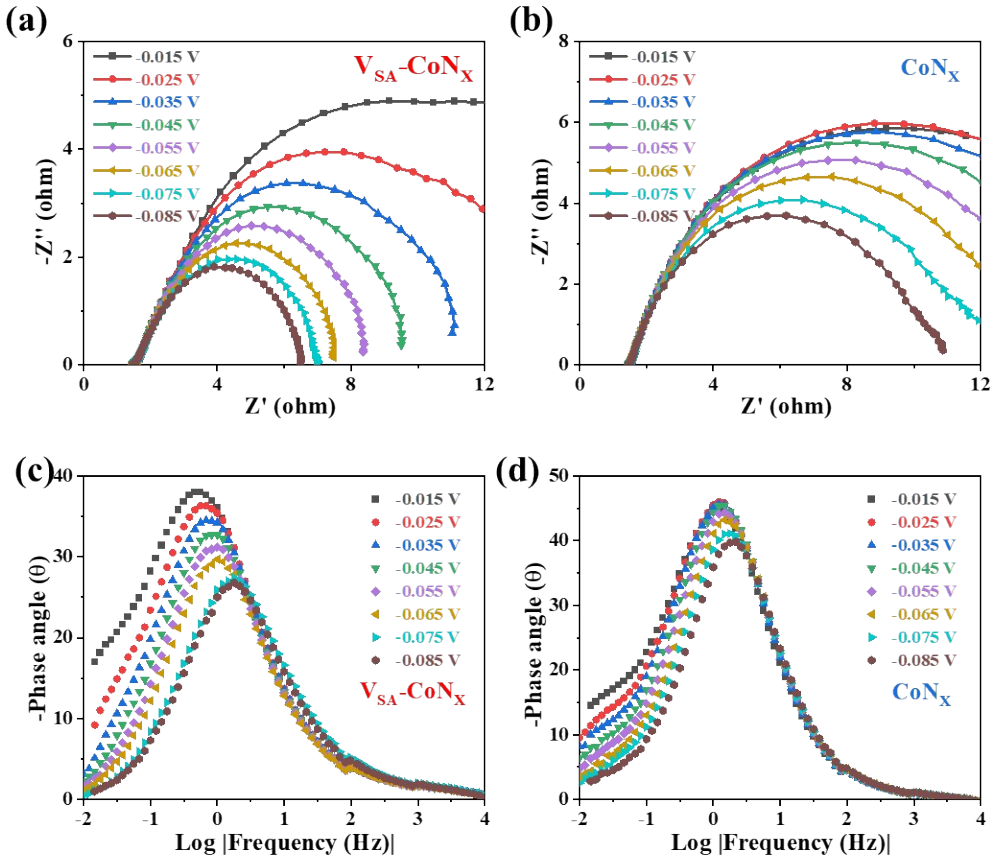

Figure S24. Nyquist plots of a) V_{SA}-CoN_X and b) CoN_X at different voltages. Bode phase plots of c) V_{SA}-CoN_X and d) CoN_X at different voltages.

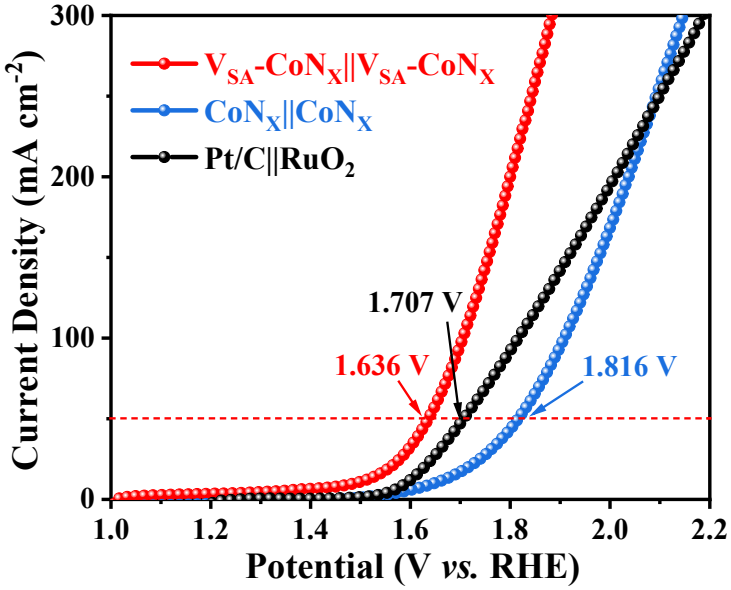

Figure S25. LSV curves of water electrolysis for the V_{SA}-CoN_X||V_{SA}-CoN_X, Pt/C|RuO_2 and CoN_X||CoN_X.

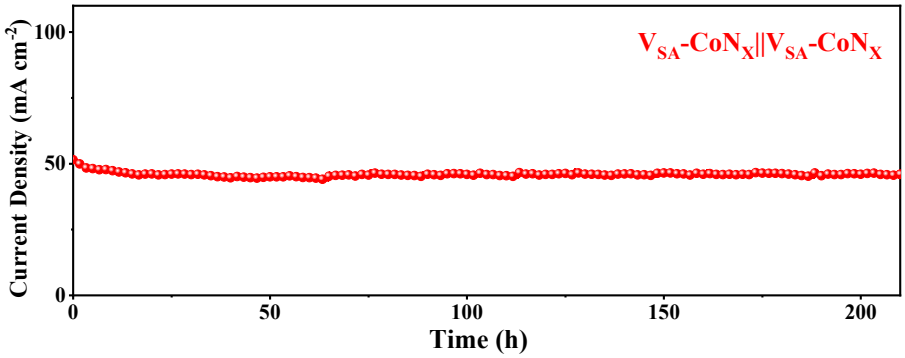

Figure S26. The stability test for V_{SA}-CoN_X||V_{SA}-CoN_X.

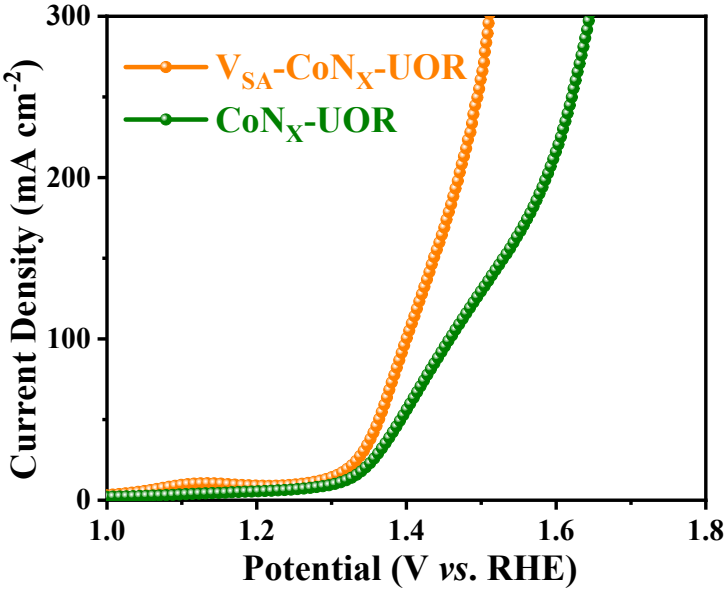

Figure S27. LSV curves of V_{SA}-CoN_X and CoN_X in 1 M KOH containing 0.5 M urea.

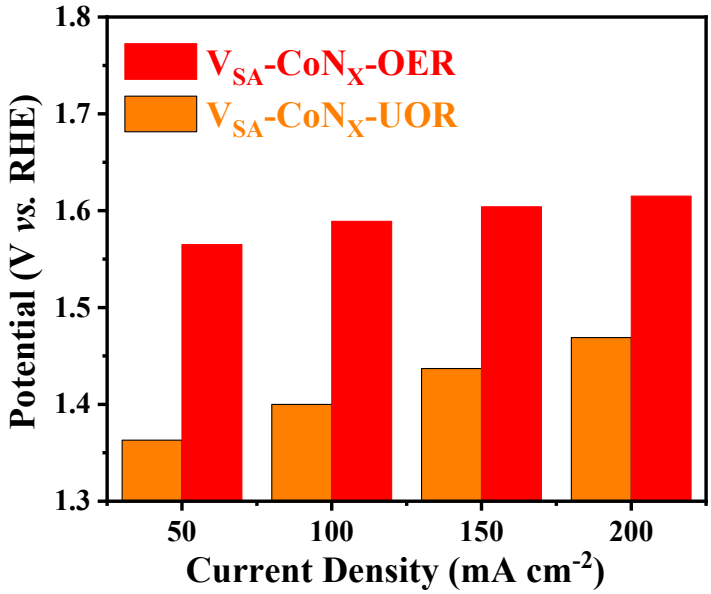

Figure S28. Driving potentials at different current densities for OER and UOR.

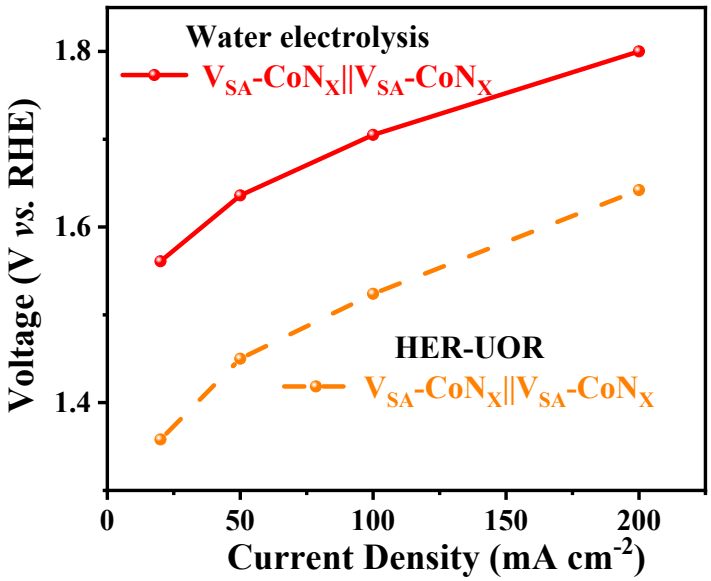

Figure S29. Driving potentials at different current densities for water and urea electrolysis.

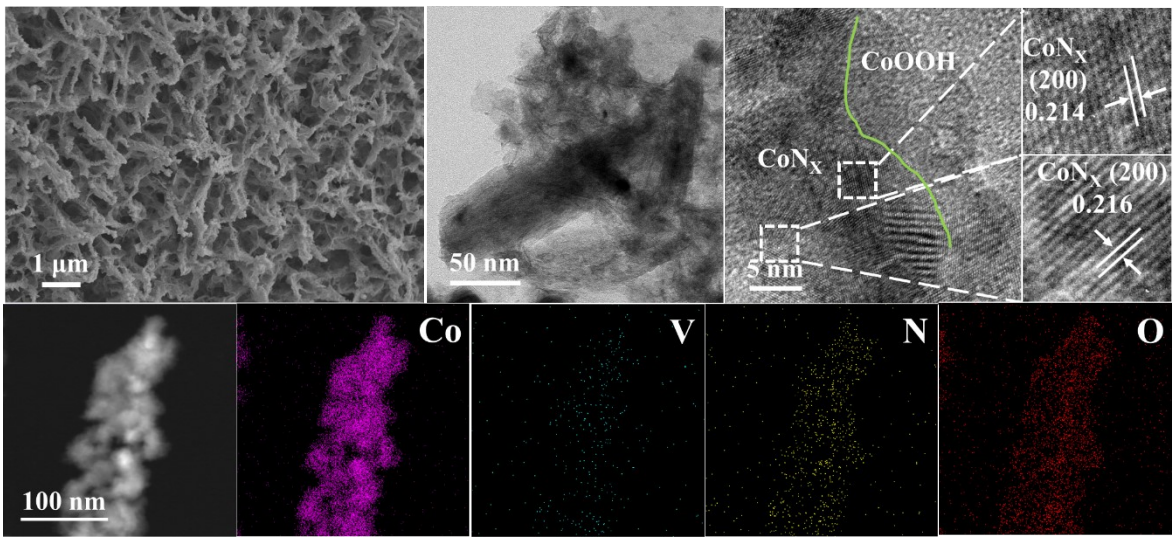

Figure S30. Characterizations of V_{SA}-CoN_X after UOR stability test.

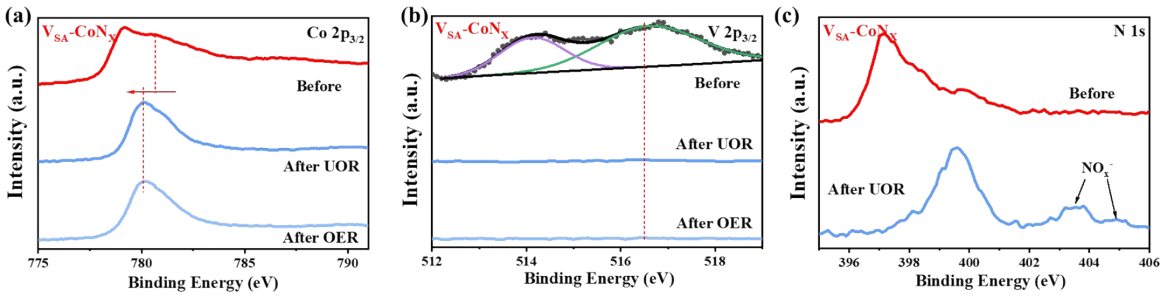

Figure S31. XPS of V_{SA}-CoN_X before and after UOR stability test.

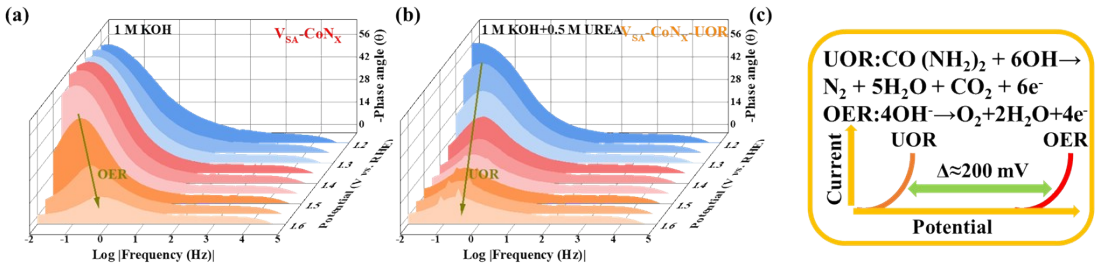

Figure S32. Bode phase plots of V_{SA}-CoN_X at different voltages for a) OER and b) UOR. c) Schematic diagram of hydrogen production by UOR instead of OER coupling.

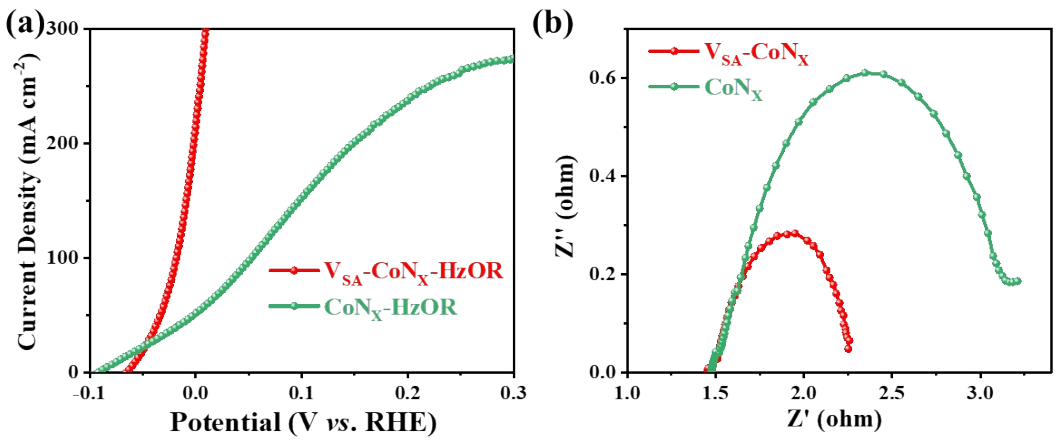

Figure S33. a) LSV curves of V_{SA}-CoN_X and CoN_X in 1 M KOH containing 0.3 M N_2H_4. b) Nyquist plots of V_{SA}-CoN_X and CoN_X.

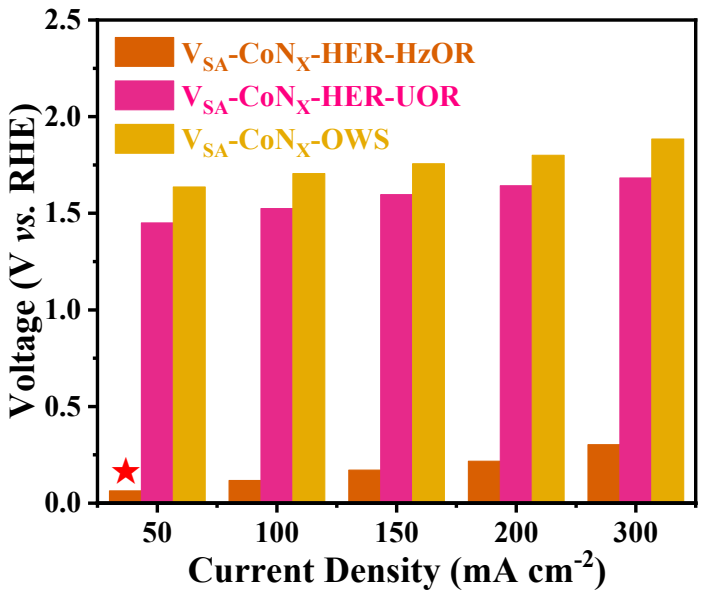

Figure S34. Driving potentials at different current densities of V_{SA}-CoN_X for OWS, HER-UOR and HER-HzOR.

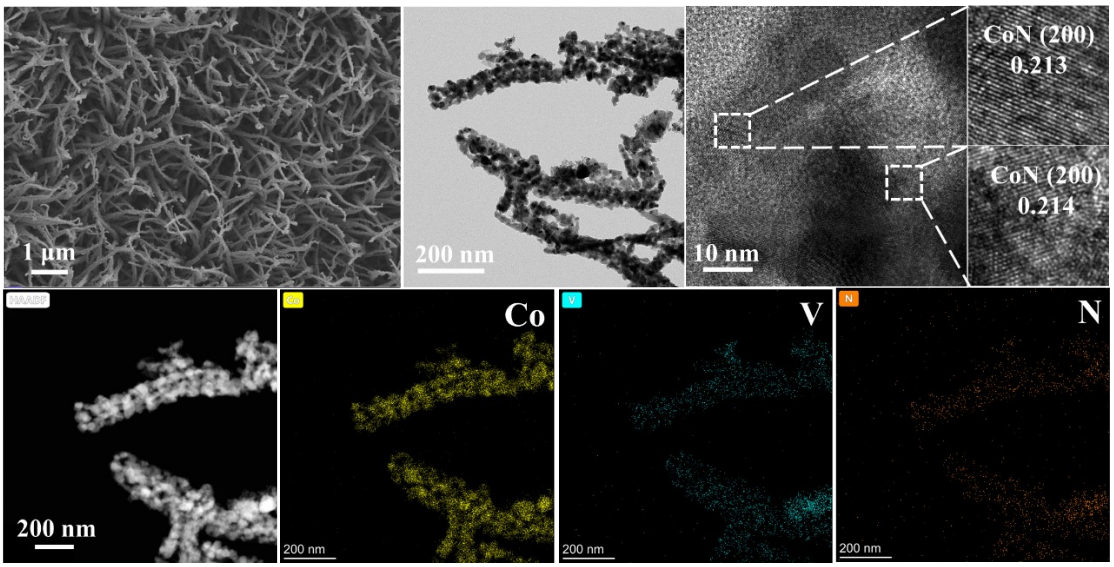

Figure S35. Characterizations of V_{SA}-CoN_X after HzOR stability test.

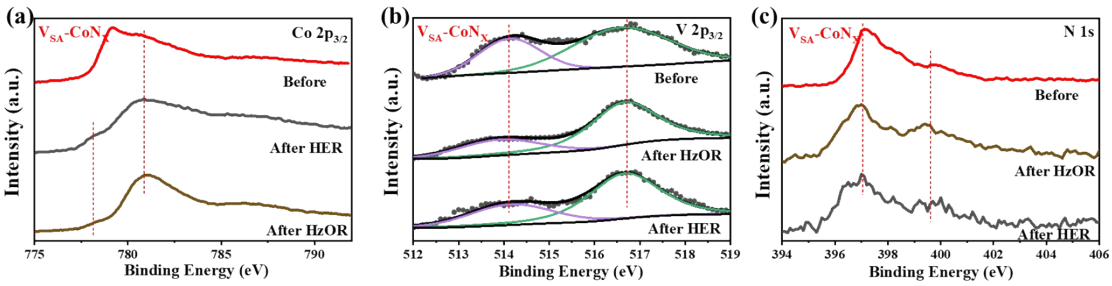

Figure S36. XPS of V_{SA}-CoN_X before and after HzOR stability test.

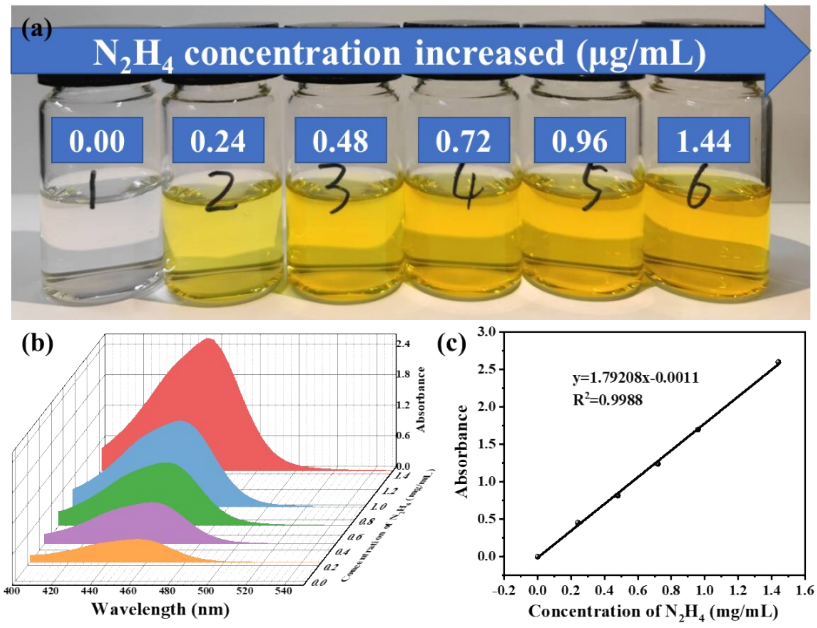

Figure S37. a) Optical image of the standard N_2H_4 solution with various concentrations used. b) UV-vis absorption spectra for above samples. c) calibration curve of the colorimetric N_2H_4 assay by the Watt and Chrisp method.

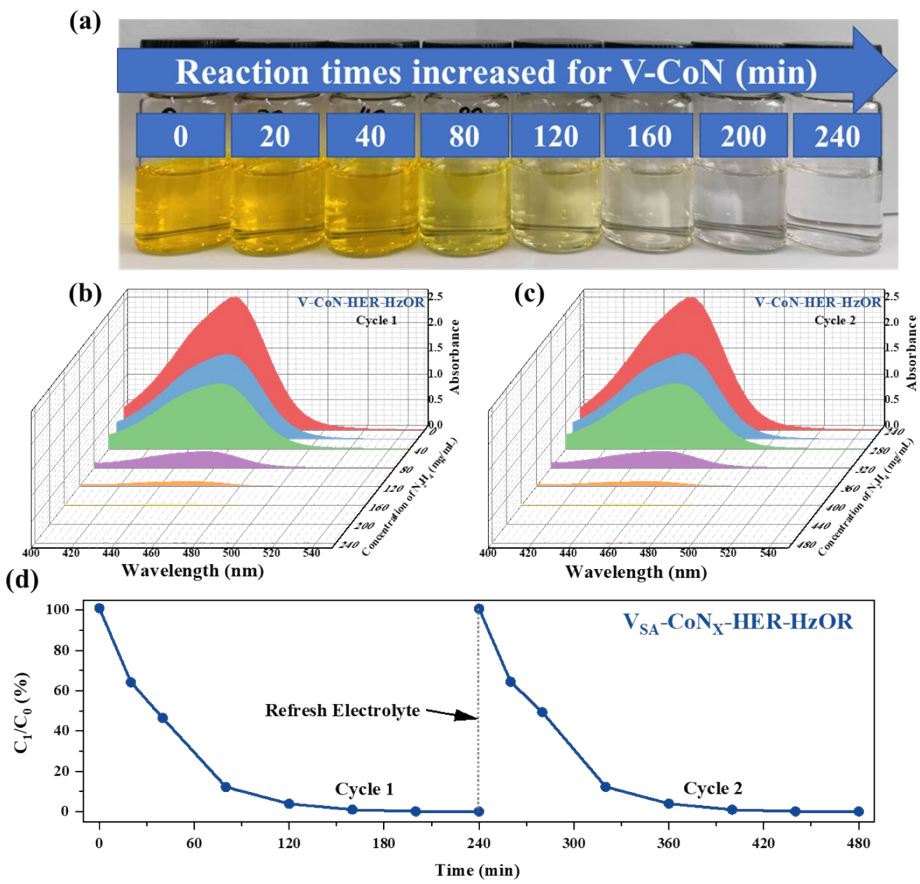

Figure S38. a) The color of electrolytes contains N_2H_4 at different time, The UV–vis spectra b) cycle 1 and c) cycle 2. c) Degradation of hydrazine electrolyte under two cycles.

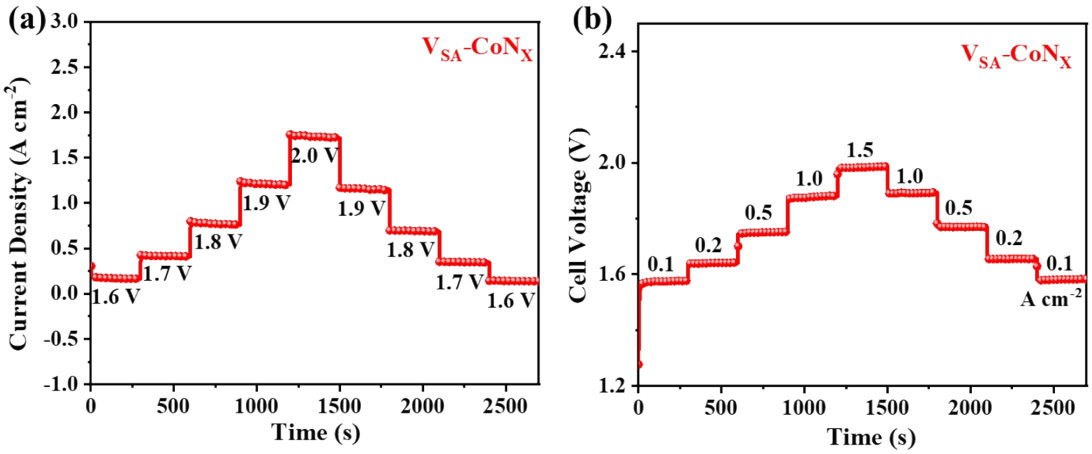

Figure S39. The a) multi-current steps and b) multi-potential steps responses curve of V_{SA}-CoN_X for AEMWE.

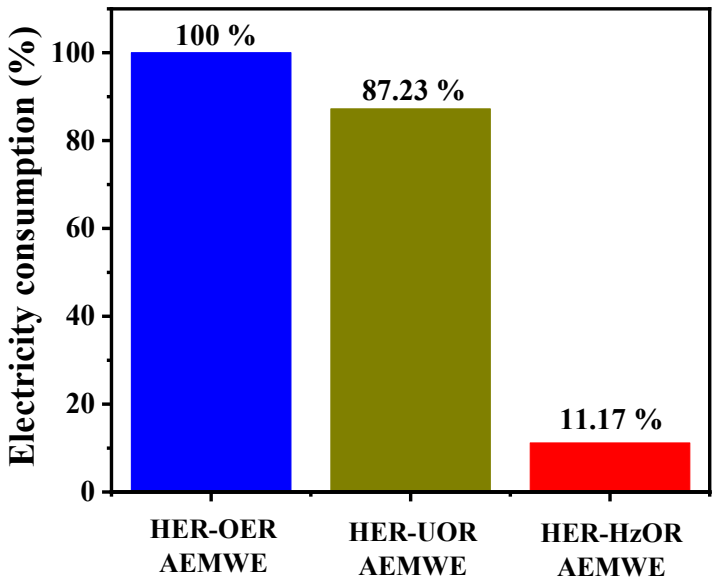

Figure S40. The AEMWE, AEMWE-UOR and AEMWE-HzOR energy consumption percentage.

Table S1. The transfer resistances obtained from Nyquist plots in 1.0 M KOH solution for HER.

Samples	R_s/Ω	R_{ct1}/Ω	R_{ct2}/Ω	R_{ct3}/Ω	$R_{ct1}+R_{ct2}+R_{ct3}/\Omega$
V_{SA}-CoN_X	1.51	3.09	1.95	0.32	5.36
CoN_X	1.49	6.96	3.25	0.37	10.58

Table S2. The water electrolysis performance of V_{SA}-CoN_X and other bifunctional HER/OER catalysts reported thus far.

Electrocatalyst	HER η (mV)@j (mA/cm^2)	OER η (mV)@j (mA/cm^2)	OWS E (V)@j (mA/cm^2)	References
V_{SA}-CoN_X	36@10	335@50	1.636@50	This work
RuO_2-Co_3O_4	90@10	152@10	1.460@10	[1]
RuO_{2-x}-$RuSe_2$	10@10	255@10	1.496@10	[2]
Fe_2O_3-CeO_2	-	172@10	1.610@100	[3]
Fe-Co-O/Co@NC-mNS	112@10	257@10	1.580@10	[4]
Ni_3N-NiMoN	31@10	277@10	1.540@10	[5]
NiMoN nanosheets	191@10	202@10	1.580@10	[6]
WS_2/Ni_3FeN	84@10	240@100	1.540@10	[7]
P-Mo-Co_3O_4@CC	-	276@10	1.540@10	[8]
$Fe_{0.33}$-Co_9S_8@SNOPC	258@10	275@10	1.595@10	[9]
Co-OSP	132@10	175@10	1.480@10	[10]
$Ce_{0.2}$-CoP/Ni_3P@NF	185@500	-	1.770@500	[11]
$Ni_{0.85}Se$-$MoSe_2$	108@10	380@10	1.700@10	[12]
NiFe/$Co(PO_3)_2$	79@10	266@10	1.630@10	[13]
N-doped Fe_2O_3/$NiTe_2$	70@10	253@10	1.540@10	[14]
$CoTe_2$-WTe_2	178@10	184@10	1.520@10	[15]

Table S3. The UOR and HER-UOR performance of V_{SA}-CoN_X and other catalysts reported thus far.

Electrocatalyst	Electrolyte	UOR E (V)@j (mA/cm^2)	HER-UOR E (V)@j (mA/cm^2)	References
V_{SA}-CoN_X	1 M KOH+0.5 M U	1.363@50	1.405@50	This work
W-NT@NF-1	1 M KOH+0.33 M U	1.390@50	1.510@10	[16]
CoFeCr LDH/NF	1 M KOH+0.33 M U	1.305@10	1.329@10	[17]
Fe-Ni_3S_2	1 M KOH+0.5 M U	1.428@100	1.570@100	[18]
NiCoCr-LDH/NF	1 M KOH+0.5 M U	1.380@100	1.427@10	[19]
NF/NiMoO-Ar	1 M KOH+0.5 M U	1.370@10	1.380@10	[20]
Ni_3S_2	1 M KOH+0.5 M U	1.339@100	1.352@10	[21]
Ni-SO_X	1 M KOH+0.33 M U	1.650@323.4	-	[22]
P-$CoNi_2S_4$ YSSs	1 M KOH+0.5 M U	1.306@10	1.544@10	[23]
Pt-Ni_2P	1 M KOH+0.33 M U	1.38@100	-	[24]
Rh/NiV-LDH	1 M KOH+0.33 M U	1.33@10	1.336@10	[25]
NiCo-BDC-S-6	1 M KOH+0.33 M U	1.326@10	-	[26]
$NiSe_2$-$NiMoO_4$/NF;	1 M KOH+0.5 M U	1.35@100	1.42@50	[27]
CoSx/Co-MOF	1 M KOH+0.5 M U	1.315@10	1.48@10	[28]

Table S4. The hydrazine electrolysis performance of V_{SA}-CoN_X and other catalysts reported thus far.

Electrocatalyst	Electrolyte	HzOR E (mV)@j (mA/cm^2)	OHzS E (V)@j (mA/cm^2)	References
V_{SA}-CoN_X	1 M KOH+0.3 M H	-33@50	0.064@50 0.117@100 0.171@150 0.214@200 0.302@300	This work
Cu_4N/Ni_3N	1 M KOH+0.5 M H	0.5@10	0.24@10	[29]
6W–O–CoP/NF	1 M KOH+0.1 M H	78.99@1000	0.0087@10	[30]
Cu_1Co_2–Ni_2P/NF	1 M KOH+0.1 M H	-50@10	0.16@10 0.39@100	[31]
Pt@NiFc-MOF	1 M KOH+0.5 M H	357@1500	0.518@1500	[32]
Ru_1-NiCoP	1 M KOH+0.3 M H	-60@10	0.09@50 0.14@100 0.17@150 0.193@200	[33]
Ru_c/NiFe-LDH	1 M KOH+0.3 M H	-75@10	0.03@10 0.29@100 0.68@300 1.03@500	[34]
PW-Co_3N	1 M KOH+0.1 M H	-55@10	0.358@10 0.428@50 0.501@100 0.607@200	[35]
NiMo/Ni_2P	1 M KOH+0.5 M H	-17@10	0.181@100 0.343@500	[36]
RuP/PNPC	1 M KOH+0.5 M H	-83@10	0.011@10 0.145@50	[37]

Table S5. The performance of V_{SA}-CoN_X and other catalysts reported thus far for AEMWE.

Electrocatalyst	Electrolyte	Performance E (V)@j (A/cm^2)	References
V_{SA}-CoN_X|| V_{SA}-CoN_X	1 M KOH 1 M KOH+0.5 M U 1 M KOH+0.3 M H	1.88@1 1.64@1 0.21@1	This work
Nei-Ir_1/CoGaOOH ||Pt/C	1 M KOH	2.1@1	[38]
AgSAs&NPs@CoO(O)H ||Pt/C	1 M KOH	1.98@1	[39]
NA-Ru_3Ni/C ||NA-Ru_3Ni/C	1 M KOH	2.048@1	[40]
Ni||Ni	1 M KOH	1.9@0.15	[41]
Fe-NiMo-NH_3/H_2 ||NiMo-NH_3/H_2	1 M KOH	1.57@1	[42]
VO_x-CoP|| VO_x-CoP	1 M KOH 1 M KOH+0.3 M U	~1.9@0.3 1.77@0.3	[42]
Ru_c/NiFe-LDH	1 M KOH 1 M KOH+0.3 M H	2.08@1 0.43@1	[34]
Ni-SN@C	1 M KOH+0.3 M H (seawater)	0.7@1	[43]
CC@CoNC (H-cell)	1 M KOH 1 M KOH+0.5 M H	2.04@0.2 0.557@0.2	[44]
MoNi (H-cell)	1 M KOH 1 M KOH+0.5 M H (seawater)	2.05@1 0.54@1	[45]

Table S6. EXAFS fitting parameters at the Co K–edge for various samples.

Sample	Path	CN	**R(Å)**	**σ^2/Å^2**	***R* factor**
Co foil	Co-Co	12.0	2.49	0.006	0.003
CoO	Co-O	5.8	2.10	0.011	0.007
	Co-Co	12.0	3.01	0.009	
CoN_X	Co-N	0.6	1.97	0.009	0.016
	Co-Co	4.5	2.50	0.006	
V_{SA}-CoN_X	Co-N	0.6	2.02	0.009	0.015
	Co-Co	4.1	2.48	0.006	
	Co-V	0.8	2.61	0.002	

CN, coordination number; R, distance between absorber and backscatter atoms; σ^2, Debye-Waller factor to account for both thermal and structural disorders; R factor indicates the goodness of the fit. Fitting range: 3.0 < k (/Å) < 12 and 1.0 < R (Å)< 3.0; A reasonable range of EXAFS fitting parameters: 0.600 < S_0^2 < 1.000; CN > 0; σ^2 > 0 Å^2; R factor < 0.02.

Table S7. The element compositions of catalysts in 1 cm^2 of V_{SA}-CoN_X before and after HzOR estimated from ICP measurements.

V_{SA}-CoN_X	**Mass (mg)**	**Co(wt%)**	**n (Co) (mmol)**	**V(wt%)**	**n (V) (mmol)**
Before	29.4	8.77	0.044	1.67	0.010
After	28.3	8.13	0.039	1.53	0.009

References

[1] Y. Jiang, H. Liu, Y. Jiang, Y. Mao, W. Shen, M. Li, R. He, *Applied Catalysis B: Environmental* **2023**, 324, 122294.

[2] Y. Chen, Y. Liu, L. Li, T. Sakthive, Z. Guo, Z. Dai, *Advanced Functional Materials* **2024**, 2406587.

[3] Q. Huang, G.-J. Xia, B. Huang, D. Xie, J. Wang, D. Wen, D. Lin, C. Xu, L. Gao, Z. Wu, J. Wu, F. Xie, W. Guo, R. Zou, *Energy & Environmental Science* **2024**.

[4] T. I. Singh, G. Rajeshkhanna, U. N. Pan, T. Kshetri, H. Lin, N. H. Kim, J. H. Lee, *Small* **2021**, 17, 2101312.

[5] A. Wu, Y. Xie, H. Ma, C. Tian, Y. Gu, H. Yan, X. Zhang, G. Yang, H. Fu, *Nano Energy* **2018**, 44, 353.

[6] Y. Zhang, B. Zhang, Z. Yin, X. Ma, Y. Zhou, *New Journal of Chemistry* **2022**, 46, 11893.

[7] J. Zeng, L. Zhang, Q. Zhou, L. Liao, Y. Qi, H. Zhou, D. Li, F. Cai, H. Wang, D. Tang, F. Yu, *Small* **2021**, 18, 2104624.

[8] Y. Huang, M. Li, F. Pan, Z. Zhu, H. Sun, Y. Tang, G. Fu, *Carbon Energy* **2022**, 5, e279.

[9] J. Khan, H. Liu, J. Xiao, Y. Zhu, A. Hayat, H. Ullah, G. Ahmed, H. Zhang, Y. Sun, L. Han, *Journal of Physics and Chemistry of Solids* **2023**, 175, 111220.

[10] B. Chong, M. Xia, Y. Lv, H. Li, X. Yan, B. Lin, G. Yang, *Chemical Engineering Journal* **2023**, 465, 142853.

[11] F. Zhang, X. Wang, W. Han, Y. Qian, L. Qiu, Y. He, L. Lei, X. Zhang, *Advanced Functional Materials* **2022**, 33, 2212381.

[12] H. R. Inta, S. Ghosh, A. Mondal, G. Tudu, H. V. S. R. M. Koppisetti, V. Mahalingam, *ACS Applied Energy Materials* **2021**, 4, 2828.

[13] F. Gu, Q. Zhang, X. H. Chen, T. Li, H. C. Fu, H. Q. Luo, N. B. Li, *International Journal of Hydrogen Energy* **2022**, 47, 28475.

[14] W. Li, Y. Deng, L. Luo, Y. Du, X. Cheng, Q. Wu, *Journal of Colloid and Interface Science* **2023**, 639, 416.

[15] M. Velpandian, A. Ragunathan, G. Ummethala, S. R. Krishna Malladi, P. Meduri, *ACS Applied Energy Materials* **2023**, 6, 5968.

[16] M. Liu, W. Zou, S. Qiu, N. Su, J. Cong, L. Hou, *Advanced Functional Materials* **2023**, 34, 2310155.

[17] Z. Wang, W. Liu, Y. Hu, M. Guan, L. Xu, H. Li, J. Bao, H. Li, *Applied Catalysis B: Environmental* **2020**, 272, 118959.

[18] D. Li, W. Wan, Z. Wang, H. Wu, S. Wu, T. Jiang, G. Cai, C. Jiang, F. Ren, *Advanced Energy Materials* **2022**, 12, 2201913.

[19] S. Xu, D. Jiao, X. Ruan, Z. Jin, Y. Qiu, Z. Feng, L. Zheng, J. Fan, W. Zheng, X. Cui, *Advanced Functional Materials* **2024**, 2401265.

[20] Z.-Y. Yu, C.-C. Lang, M.-R. Gao, Y. Chen, Q.-Q. Fu, Y. Duan, S.-H. Yu, *Energy & Environmental Science* **2018**, 11, 1890.

[21] Z. Xiao, Y. Qian, T. Tan, H. Lu, C. Liu, B. Wang, Q. Zhang, M. T. Sarwar, R. Gao, A. Tang, H. Yang, *Journal of Materials Chemistry A* **2023**, 11, 259.

[22] X. Gao, X. Bai, P. Wang, Y. Jiao, K. Davey, Y. Zheng, S.-Z. Qiao, *Nature Communications* **2023**, 14, 5842.

[23] X. F. Lu, S. L. Zhang, W. L. Sim, S. Gao, X. W. Lou, *Angewandte Chemie International Edition* **2021**, 60, 22885.

[24] J. Zhang, J. Feng, J. Zhu, L. Kang, L. Liu, F. Guo, J. Li, K. Li, J. Chen, W. Zong, M. Liu, R. Chen, I. P. Parkin, L. Mai, G. He, *Angewandte Chemie International Edition* **2024**.

[25] H. Sun, L. Li, H.-C. Chen, D. Duan, M. Humayun, Y. Qiu, X. Zhang, X. Ao, Y. Wu, Y. Pang, K. Huo, C. Wang, Y. Xiong, *Science Bulletin* **2022**, 67, 1763.
[26] X. Ao, Y. Gu, C. Li, Y. Wu, C. Wu, S. Xun, A. Nikiforov, C. Xu, J. Jia, W. Cai, R. Ma, K. Huo, C. Wang, *Applied Catalysis B: Environmental* **2022**, 315, 121586.
[27] T. Yu, Q. Xu, J. Chen, G. Qian, X. Zhuo, H. Yang, S. Yin, *Chemical Engineering Journal* **2022**, 449, 137791.
[28] H. Xu, K. Ye, K. Zhu, J. Yin, J. Yan, G. Wang, D. Cao, *Inorganic Chemistry Frontiers* **2020**, 7, 2602.
[29] Z. Wang, L. Xu, F. Huang, L. Qu, J. Li, K. A. Owusu, Z. Liu, Z. Lin, B. Xiang, X. Liu, K. Zhao, X. Liao, W. Yang, Y. B. Cheng, L. Mai, *Advanced Energy Materials* **2019**, 9, 1900390.
[30] G. Meng, Z. Chang, L. Zhu, C. Chen, Y. Chen, H. Tian, W. Luo, W. Sun, X. Cui, J. Shi, *Nano-Micro Letters* **2023**, 15, 212.
[31] C. Feng, M. L. , J. S. , H. W. , W. Z. , S. Q. , C. D. , X. C. , H. Y. , Q. H. , Chuanxin Hea, *Advanced Materials* **2023**, 2305598.
[32] Y. Huang, X. Zhang, L. Li, M. Humayun, H. Zhang, X. Xu, S. P. Anthony, Z. Chen, J. Zeng, D. V. Shtansky, K. Huo, H. Song, C. Wang, W. Zhang, *Advanced Functional Materials* **2024**, 2401011.
[33] Y. Hu, T. Chao, Y. Li, P. Liu, T. Zhao, G. Yu, C. Chen, X. Liang, H. Jin, S. Niu, W. Chen, D. Wang, Y. Li, *Angewandte Chemie International Edition* **2023**, 62, e202308800.
[34] Y. Zhu, Y. Chen, Y. Feng, X. Meng, J. Xia, G. Zhang, *Advanced Materials* **2024**, 2401694.
[35] Y. Liu, J. Zhang, Y. Li, Q. Qian, Z. Li, Y. Zhu, G. Zhang, *Nature Communications* **2020**, 11, 1853.
[36] Y. Yang, X. Li, G. Liu, H. Liu, Y. Shi, C. Ye, Z. Fang, M. Ye, J. Shen, *Advanced Materials* **2023**, 36, 2307979.
[37] X. Guan, Y. Sun, S. Zhao, H. Li, S. Zeng, Q. Yao, R. Li, H. Chen, K. Qu, *SusMat* **2024**, 4, 166.
[38] P. Ma, H. Cao, Q. Hao, R. Wang, W. Liu, M. Zuo, C. Jia, Z. Zhang, J. Bao, *Angewandte Chemie International Edition* **2024**, e202404418.
[39] X. Guo, H. Zhang, W. Xia, M. Ma, D. Cao, D. Cheng, *Advanced Functional Materials* **2024**, 2316539.
[40] F. B. Lei Gao, Xin Tan, Mengfan Li, Zhen Shen, Xuli Chen, Ziyi Tang, Wenchuan Lai, Yangfan Lu, Peifeng Huang, Chao Ma,, Z. Y. Sean C. Smith, Zheng Hu and Hongwen Huang, *Energy & Environmental Science* **2023**, 16, 285.
[41] S. H. Ahn, B.-S. Lee, I. Choi, S. J. Yoo, H.-J. Kim, E. Cho, D. Henkensmeier, S. W. Nam, S.-K. Kim, J. H. Jang, *Applied Catalysis B: Environmental* **2014**, 154-155, 197.
[42] P. Chen, X. Hu, *Advanced Energy Materials* **2020**, 10, 2002285.
[43] H. Jin, X. Wang, C. Tang, A. Vasileff, L. Li, A. Slattery, S. Z. Qiao, *Advanced Materials* **2021**, 33, 2007508.
[44] Y. Xin, K. Shen, T. Guo, L. Chen, Y. Li, *Small* **2023**, 19, 2300019.
[45] L. Guo, Q. Yu, X. Zhai, J. Chi, T. Cui, Y. Zhang, J. Lai, L. Wang, *Nano Research* **2022**, 15, 8846.